



Emergent Collective Chemotaxis without Single-Cell Gradient Sensing

Brian A. Camley,¹ Juliane Zimmermann,² Herbert Levine,^{2,3} and Wouter-Jan Rappel¹

¹*Department of Physics, University of California, San Diego, La Jolla, California 92093, USA*

²*Center for Theoretical Biological Physics, Rice University, Houston, Texas 77005, USA*

³*Department of Bioengineering, Rice University, Houston, Texas 77005, USA*

(Received 18 September 2015; published 3 March 2016)

Many eukaryotic cells chemotax, sensing and following chemical gradients. However, experiments show that even under conditions when single cells cannot chemotax, small clusters may still follow a gradient. This behavior is observed in neural crest cells, in lymphocytes, and during border cell migration in *Drosophila*, but its origin remains puzzling. Here, we propose a new mechanism underlying this “collective guidance,” and study a model based on this mechanism both analytically and computationally. Our approach posits that contact inhibition of locomotion, where cells polarize away from cell-cell contact, is regulated by the chemoattractant. Individual cells must measure the mean attractant value, but need not measure its gradient, to give rise to directional motility for a cell cluster. We present analytic formulas for how the cluster velocity and chemotactic index depend on the number and organization of cells in the cluster. The presence of strong orientation effects provides a simple test for our theory of collective guidance.

DOI: 10.1103/PhysRevLett.116.098101

Cells often perform chemotaxis, detecting and moving toward increasing concentrations of a chemoattractant, to find nutrients or reach a targeted location. This is a fundamental aspect of biological processes from immune response to development. Many single eukaryotic cells sense gradients by measuring how a chemoattractant varies over their length [1]; this is distinct from bacteria that measure chemoattractant over time [2]. In both, single cells have a net motion toward higher chemoattractant.

Recent measurements of how neural crest cells respond to the chemoattractant Sdf1 suggest that single neural crest cells cannot chemotax effectively, but small clusters can [3]. A more recent experimental and theoretical study shows that at low gradients, clusters of lymphocytes also chemotax without corresponding single cell directional behavior; at higher gradients clusters actually move oppositely to single cells [4]. Late border cell migration in the *Drosophila* egg chamber may also occur by a similar mechanism [5–8]. These experiments strongly suggest that gradient sensing in a cluster of cells may be an emergent property of cell-cell interactions, rather than arising from amplifying a single cell’s biased motion; interestingly, some fish schools also display emergent gradient sensing [9]. In fact, these experiments led to a “collective guidance” hypothesis [6], in which a cluster of cells where each individual cell has no information about the gradient may nevertheless move directionally (see also [4] for a related model). In a sense that will become clear, cell-cell interactions allow for a measurement of the gradient across the entire cluster, as opposed to across a single cell.

In this Letter, we develop a quantitative model that embodies the collective guidance hypothesis. Our model is based on modulation of the well-known contact inhibition

of locomotion (CIL) interaction [10–12], in which cells move away from neighboring cells. We propose that individual cells measure the local signal concentration and adjust their CIL strength accordingly; the cluster moves directionally due to the spatial bias in the cell-cell interaction. We discuss the suitability of this approach for explaining current experiments, and provide experimental criteria to distinguish between chemotaxis via collective guidance and other mechanisms where clusters could gain improvement over single-cell migration [13,14]. These results may have relevance to collective cancer motility [15], as recent data suggest that tumor cell clusters are particularly effective metastatic agents [16].

We consider a cluster of cells exposed to a chemical gradient $S(\mathbf{r})$. We use a two-dimensional stochastic particle model to describe cells, giving each cell i a position \mathbf{r}^i and a polarity \mathbf{p}^i . The cell polarity indicates its direction and propulsion strength: an isolated cell with polarity \mathbf{p}^i has velocity \mathbf{p}^i . The cell’s motion is overdamped, so the cell’s velocity is \mathbf{p}^i plus the total physical force other cells exert on it, $\sum_{j \neq i} \mathbf{F}^{ij}$. Biochemical interaction between cells alter a cell’s polarity \mathbf{p}^i . Our model is then

$$\partial_t \mathbf{r}^i = \mathbf{p}^i + \sum_{j \neq i} \mathbf{F}^{ij}, \quad (1)$$

$$\partial_t \mathbf{p}^i = -\frac{1}{\tau} \mathbf{p}^i + \sigma \boldsymbol{\xi}^i(t) + \beta^i \sum_{j \sim i} \hat{\mathbf{r}}^{ij}, \quad (2)$$

where the \mathbf{F}^{ij} are intercellular forces of cell-cell adhesion and volume exclusion, and the $\boldsymbol{\xi}^i(t)$ are Gaussian Langevin noises with $\langle \xi_\mu^i(t) \xi_\nu^j(t') \rangle = 2\delta_{\mu\nu} \delta^{ij} \delta(t-t')$. Greek indices μ, ν run over the dimensions x, y . The first two terms on the

right of Eq. (2) are a standard Ornstein-Uhlenbeck model [17,18]: \mathbf{p}^i relaxes to zero with time scale τ , but is driven away from zero by the noise $\xi(t)$. This corresponds with a cell that is orientationally persistent over time τ .

We introduce the last term in Eq. (2) to describe CIL. CIL is a well-known property of many cell types in which cells polarize away from cell-cell contact [11,12,19–21]. We model CIL by biasing \mathbf{p}^i away from nearby cells, toward $\mathbf{q}^i = \sum_{j \sim i} \hat{\mathbf{r}}^{ij}$, where $\hat{\mathbf{r}}^{ij} = (\mathbf{r}^i - \mathbf{r}^j)/|\mathbf{r}^i - \mathbf{r}^j|$ is the unit vector pointing from cell j to cell i and the sum over $j \sim i$ indicates the sum over the neighbors of i (those cells within a distance $D_0 = 1.2$ cell diameters). While this is motivated by CIL in neural crest cells, it is also a natural minimal model under the assumption that cells know nothing about their neighbors other than their direction $\hat{\mathbf{r}}^{ij}$. For cells along the cluster edge, the CIL bias \mathbf{q}^i points outward, but for interior cells \mathbf{q}^i is smaller or zero [Fig. 1(a)]. This is consistent with experimental observations that edge cells have a strong outward polarity, while interior cells have weaker protrusions [3].

Chemotaxis arises in our model if the chemoattractant $S(\mathbf{r})$ changes a cell's susceptibility to CIL, β^i ; $\beta^i = \bar{\beta}S(\mathbf{r}^i)$. This models the result of Ref. [3] that the chemoattractant Sdf1 stabilizes protrusions induced by CIL [3]. We also assume the cell's chemotactic receptors are not close to saturation—i.e., the response is perfectly linear. If CIL occurs without chemoattractant ($S = 0$), as in neural crest cells [3], i.e., $\beta^i = \beta_0 + \bar{\beta}S(\mathbf{r})$, this will not significantly change our analysis, only shifting the strength of CIL at the origin. Similar results are obtained if all protrusions are stabilized by Sdf1 (τ regulated by S), though with complications (Supplemental Material [22], Fig. S1).

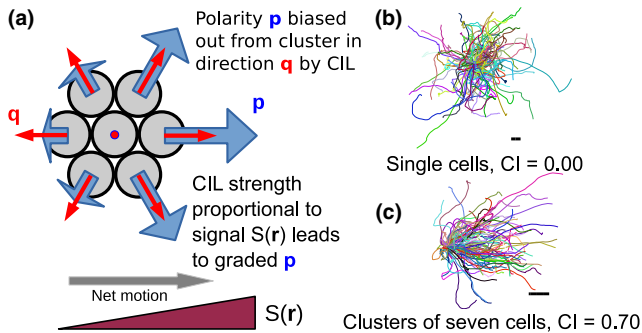


FIG. 1. Signal-dependent contact inhibition of locomotion creates directed motion. (a) Schematic picture of the model and origin of directed motion. Cell polarities are biased away from the cluster toward the direction $\mathbf{q}^i = \sum_{j \sim i} \hat{\mathbf{r}}^{ij}$ by contact inhibition of locomotion (CIL); the strength of this bias is proportional to the local chemoattractant value $S(\mathbf{r})$, leading to cells being more polarized at higher S . See the text for details. (b) One hundred trajectories of a single cell and (c) a cluster of seven cells. Trajectories are six persistence times in length (120 min). Scale bar is one cell diameter. The gradient strength $|\nabla S| = 0.025$, with the gradient in the x direction.

Analytic predictions for cluster velocity.—Our model predicts that while single cells do not chemotax, clusters as small as two cells will, consistent with Ref. [3]. We can analytically predict the mean drift of a cluster of cells obeying Eqs. (1) and (2):

$$\langle \mathbf{V} \rangle_c \approx \bar{\beta} \tau \mathcal{M} \cdot \nabla S, \quad (3)$$

where the approximation is true for shallow gradients $S(\mathbf{r}) \approx S_0 + \mathbf{r} \cdot \nabla S$. $\langle \dots \rangle_c$ indicates an average over the fluctuating \mathbf{p}^i but with a fixed configuration of cells \mathbf{r}^i . The matrix \mathcal{M} only depends on the cells' configuration

$$\mathcal{M}_{\mu\nu} = \frac{1}{N} \sum_i q_{\mu}^i q_{\nu}^i, \quad (4)$$

where, as above, $\mathbf{q}^i = \sum_{j \sim i} \hat{\mathbf{r}}^{ij}$. Equation (3) resembles the equation of motion for an arbitrarily shaped object in a low Reynolds number fluid under a constant force $\bar{\beta} \tau \nabla S$ [23]: by analogy, we call \mathcal{M} the “mobility matrix.” There is, however, no fluctuation-dissipation relationship as there would be in equilibrium [24].

To derive Eq. (3), we note that in our units the velocity of a single cell is equal to the force on it; i.e., the mobility is one [Eq. (1)]. For a cluster of N cells, the mean velocity of the cluster is $1/N$ times the total force on the cluster. As $\mathbf{F}^{ij} = -\mathbf{F}^{ji}$, the cluster velocity is $\mathbf{V} = N^{-1} \sum_i \mathbf{p}^i$. When the cluster configuration changes slowly over the time scale τ , Eq. (2) can be treated as an Ornstein-Uhlenbeck equation with a time-independent bias from CIL. The mean polarity is then $\langle \mathbf{p}^i \rangle = \beta^i \tau \sum_{j \sim i} \hat{\mathbf{r}}^{ij}$, with Gaussian fluctuations away from the mean, $\langle (\mathbf{p}_{\mu}^i - \langle \mathbf{p}_{\mu}^i \rangle)^2 \rangle = \sigma^2 \tau$. The mean cell cluster velocity is

$$\langle \mathbf{V} \rangle_c = \frac{\bar{\beta} \tau}{N} \sum_i S(\mathbf{r}^i) \sum_{j \sim i} \hat{\mathbf{r}}^{ij}. \quad (5)$$

In a constant chemoattractant field $S = S_0$, no net motion is observed, as $\sum_i \sum_{j \sim i} \hat{\mathbf{r}}^{ij} = 0$. For linear or slowly varying gradients $S(\mathbf{r}) \approx S_0 + \mathbf{r} \cdot \nabla S$, and we get Eq. (3).

Cluster motion and chemotactic efficiency depend on cluster size, shape, and orientation.—Within our model, a cluster's motion can be highly anisotropic. Consider a pair of cells separated by unit distance along $(\cos \theta, \sin \theta)$. Then, $\mathcal{M}_{xx} = \frac{1}{2} \cos^2 \theta$, $\mathcal{M}_{xy} = \mathcal{M}_{yx} = \frac{1}{2} \cos \theta \sin \theta$, and $\mathcal{M}_{yy} = \frac{1}{2} \sin^2 \theta$. If the gradient is in the x direction, then $\langle V_x \rangle_c = (V_0/2) \cos^2 \theta$ and $\langle V_y \rangle_c = (V_0/2) \cos \theta \sin \theta$, where $V_0 = \bar{\beta} \tau |\nabla S|$. Cell pairs move toward higher chemoattractant, but their motion is along the pair axis, leading to a transient bias in the y direction before the cell pair reorients due to fluctuations in \mathbf{p}^i (Fig. 2). We compare our theory for the motility of rigid cell clusters [Eq. (3)] with a simulation of Eqs. (1) and (2) with strongly adherent cell pairs with excellent agreement (Fig. 2).

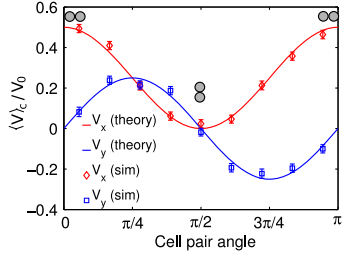


FIG. 2. Adherent pairs of cells undergo highly anisotropic chemotaxis. The average chemotactic velocity of a cell pair $\langle V_x \rangle_c$ depends strongly on the angle θ between the cell-cell axis and the chemotactic gradient. Cell pairs also drift perpendicular to the gradient; $\langle V_y \rangle_c \neq 0$. $V_0 \equiv \beta\tau|\nabla S|$ is the velocity scale; $|\nabla S| = 0.025$. Simulations are of Eqs. (1) and (2). We compute $\langle V_\mu \rangle_c$ by tracking the instantaneous angle and then averaging over all velocities within the appropriate angle bin. Error bars here and throughout are 1 standard deviation of the mean, calculated from a bootstrap. Over $n = 13000$ trajectories of 6τ (120 min) are simulated.

For the simulations in Fig. 2 and throughout the Letter, we solve the model equations (1) and (2) numerically using a standard Euler-Maruyama scheme. We choose units where the equilibrium cell-cell separation (roughly $20 \mu\text{m}$ for neural crest cells [3]) is unity, and the relaxation time $\tau = 1$ (we estimate $\tau = 20$ min in neural crest cells [3]). Within these units, neural crest cell velocities are on the order of 1. We choose $\sigma = 1$, so the root mean square speed of an isolated cell is $\langle |\mathbf{V}|^2 \rangle^{1/2} = 2^{1/2}\sigma\tau^{1/2} \approx 1.4 \mu\text{m}/\text{min}$. The cluster velocity scale is $V_0 = \beta\tau|\nabla S|$, which is 0.5 ($0.5 \mu\text{m}/\text{min}$ in physical units) if $|\nabla S| = 0.025$ and $S(0) = 1$; i.e., β^i changes by 2.5% across a cell at the origin. Cell-cell forces \mathbf{F}^{ij} are stiff springs so that clusters are effectively rigid (see the Supplemental Material [22] for details).

We can also compute \mathcal{M} and hence $\langle V_x \rangle$ for larger clusters (see Table S1 and Fig. S2 of the Supplemental Material [22]). For a cluster of Q layers of cells surrounding a center cell, $\mathcal{M}_{\mu\nu} = f(Q)\delta_{\mu\nu}$, with $f(Q) = [(9Q^2 + 3Q)/(2 + 6Q + 6Q^2)]$. A cluster with Q layers has $N = 1 + 3Q + 3Q^2$ cells; thus, the mean velocity of a Q -layer cluster is given by $\langle V_x \rangle_c / V_0 = \overline{\mathcal{M}} = [(3N - \sqrt{12N - 3})/2N]$, where $\overline{\mathcal{M}} = \frac{1}{2}(\mathcal{M}_{xx} + \mathcal{M}_{yy})$ is the angular average of \mathcal{M} . We predict that $\langle V_x \rangle_c / V_0$ first increases with N , then slowly saturates to $3/2$. This is confirmed by full model simulations [Fig. 3(a)]. We note that $\langle V_x \rangle$ is an average over time, and hence orientation (see below and the Supplemental Material [22]). We can see why $\langle V_x \rangle$ saturates as $N \rightarrow \infty$ by considering a large circular cluster of radius R . Here, we expect $\mathbf{q}^i = a\hat{\mathbf{n}}$ on the outside edge, where a is a geometric prefactor and $\hat{\mathbf{n}}$ is the outward normal, with $\mathbf{q}^i = \mathbf{0}$ elsewhere. Then, $\mathcal{M}_{\mu\nu} \sim \frac{a}{\pi R^2} \int_0^{2\pi} (Rd\theta)\hat{\mathbf{n}}_\mu(\theta)\mathbf{r}_\nu = 2a\delta_{\mu\nu}$, independent of cluster radius R . A related result has been found for circular

clusters by Malet-Engra *et al.* [4]; we note that they do not consider the behavior of single cells or cluster geometry.

The efficiency of cluster chemotaxis may be measured by the chemotactic index (CI), commonly defined as the ratio of the distance traveled along the gradient (the x displacement) to the total distance traveled [25]; the CI ranges from -1 to 1 . We define $\text{CI} \equiv \langle V_x \rangle / \langle |\mathbf{V}| \rangle$, where the average is over both time and trajectories (and hence over orientation). The chemotactic index CI may also be computed analytically, and it depends on the variance of \mathbf{V} , which is $\langle (V_x - \langle V_x \rangle)^2 \rangle = \langle (V_y - \langle V_y \rangle)^2 \rangle = \sigma^2\tau/N$. In our model, CI only depends on the ratio c of the mean chemotactic velocity to its standard deviation

$$\text{CI} = \sqrt{2/\pi}c/L_{1/2}(-c^2/2),$$

$$c = \frac{\langle V_x \rangle}{\sqrt{\langle (V_\mu - \langle V_\mu \rangle)^2 \rangle}} = \frac{\beta\tau\overline{\mathcal{M}}|\nabla S|}{\sigma\sqrt{\tau/N}}, \quad (6)$$

where $L_{1/2}$ is a generalized Laguerre polynomial. When the mean cluster velocity is much larger than its fluctuations, $c \gg 1$ and $\text{CI} \rightarrow 1$, but when fluctuations are large, $|c| \ll 1$ and $\text{CI} \rightarrow 0$ (Supplemental Material [22], Fig. S3). Together, Eqs. (3) and (6) and Table S1 [22] provide an analytic prediction for the cluster velocity and CI, with excellent agreement with simulations (Fig. 3). We note that $\langle V_x \rangle_c / V_0$ only depends on the cluster configuration, where $V_0 = \beta\tau|\nabla S|$, so $\langle V_x(N) \rangle_c / V_0$ collapses onto a single curve as the gradient strength is changed [Fig. 3(a)]. By contrast, how CI increases with N depends on $|\nabla S|$ and σ [Eq. (6), Fig. 3(b)].

In our model, clusters can in principle develop spontaneous rotation, but in practice this effect is small,

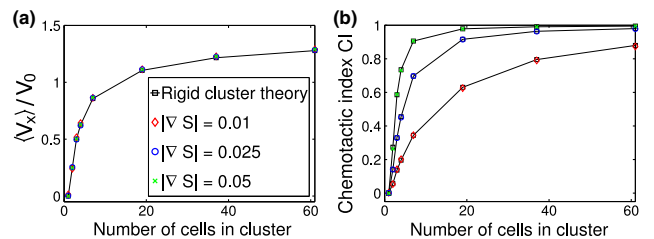


FIG. 3. Larger cell clusters chemotax more effectively, but their velocity saturates (a) As the number of cells N in a cluster increases, the mean velocity $\langle V_x \rangle_c$ increases with N but then saturates; the mean velocity can be collapsed onto a single curve by rescaling by $V_0 \equiv \beta\tau|\nabla S|$. (b) The chemotactic index CI also saturates to its maximum value. Black squares and lines are the orientationally averaged drift velocity computed for rigid clusters by Eqs. (3) and (6). Colored symbols are full model simulations with strong adhesion. Cell cluster shape may influence $\langle V_x \rangle_c$ (Supplemental Material [22], Fig. S4); our calculations are for the shapes in Table S1 [22]. Error bars here are symbol size or smaller; $n \geq 2000$ trajectories of 6τ are used for each point.

and absent for symmetric clusters (see the Supplemental Material [22]).

Motion in nonrigid clusters.—While we studied near-rigid clusters above, our results hold qualitatively for clusters that are loosely adherent and may rearrange. Cell rearrangements are common in many collective cell motions [26–29]. We choose cell-cell forces \mathbf{F}^{ij} to allow clusters to rearrange (see the Supplemental Material [22] and Ref. [30]), and simulate Eqs. (1) and (2). As in rigid clusters, $\langle V_x \rangle$ increases and saturates, while CI increases toward unity, though more slowly than a rigid cluster [Figs. 4(a) and 4(b)]. Clusters may fragment; with increasing x , β^i increases and the cluster breaks up [Fig. 4(c)]. Cluster breakup can limit guidance—if $\bar{\beta}$ is too large, the clusters are not stable. We thus decreased $\bar{\beta}$ in Fig. 4.

In Figs 4(a) and 4(b), we compute CI and the velocity by averaging over all cells, not merely those that are connected. If we track the cells ejected from the cluster, they have an apparent CI > 0 , as they are preferentially ejected from the high- β^i edge (Supplemental Material [22]). Experimental analysis of dissociating clusters may therefore not be straightforward. Anisotropic chemotaxis is present in nonrigid pairs, though lessened because they rotate quickly with respect to τ (Supplemental Material [22]).

Distinguishing between potential collective chemotaxis models.—Our model explains how chemotaxis can emerge from interactions of nonchemotaxing cells. However, other possibilities exist for enhancement of chemotaxis in clusters. Coburn *et al.* showed that in contact-based models, a few chemotactic cells can direct many nonchemotactic ones [14]. If single cells are weakly chemotactic, cell-cell interactions could amplify this response or average out

fluctuations [13]. How can we distinguish these options? In lymphocytes [4], the motion of single cells oppositely to the cluster immediately rules out simple averaging or amplification of single cell bias. More generally, the scaling of collective chemotaxis with cluster size does not allow easy discrimination. In Fig. 3, at large N , $\langle V_x \rangle$ and CI saturate. As an alternate theory, suppose each cell chemotaxes noisily, e.g., $\mathbf{p}^i = p_0 \nabla S + \mathbf{\Delta}^i$, where the $\mathbf{\Delta}$ are independent zero-mean noises. In this case, $\langle \mathbf{V} \rangle = p_0 \nabla S$ independent of N , and $\langle (V_\mu - \langle V_\mu \rangle)^2 \rangle \sim 1/N$, as in our large- N asymptotic results and the related circular-cluster theory of Ref. [4]. Instead, we propose that orientation effects in small clusters are a good test of emergent chemotaxis. In particular, studying cell pairs as in Fig. 2 is critical: anisotropic chemotaxis is a generic sign of cluster-level gradient sensing. Even beyond our model, chemotactic drift is anisotropic for almost all mechanisms where single cells do not chemotax, because two cells separated perpendicular to the gradient sense the same concentration. This leads to anisotropic chemotaxis unless cells integrate information over times much larger than the pair’s reorientation time. By contrast, the simple model with single cell chemotaxis above leads to isotropic chemotaxis of pairs.

How well does our model fit current experiments? We find increasing the cluster size increases the cluster velocity and chemotactic index. This is consistent with Ref. [4], who see an increase in taxis from small clusters (< 20 cells) to large, but not Ref. [3], who find a similar CI in small and large clusters, and note no large variations in velocity. This suggests the minimal version of collective guidance developed here can create chemotaxis, but does not fully explain the experiments of Ref. [3]. There are many directions for improvement. More quantitative comparisons could be made by detailed measurement of single-cell statistics [17,31], leading to nonlinear or anisotropic terms in Eq. (2). Our description of CIL has also assumed, for simplicity, that both the cell front and back are inhibitory; other possibilities may alter collective motility [20]. We could also add adaptation as in the Local Excitation, Global Inhibition model [32,33], enabling clusters to adapt their response to a value independent of the mean chemoattractant concentration. We will treat extensions of this model elsewhere; our focus here is on the simplest possible results.

In summary, we provide a simple, quantitative model that embodies a minimal version of the collective guidance hypothesis [3,6] and provides a plausible initial model for collective chemotaxis when single cells do not chemotax. Our work allows us to make an unambiguous and testable prediction for emergent collective guidance: pairs of cells have anisotropic chemotaxis. Although considerable effort has been devoted to models of collective motility [28,34–42], ours is the first model of how collective chemotaxis can emerge from single

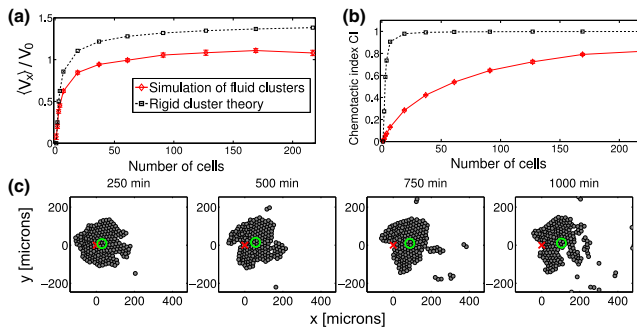


FIG. 4. Nonrigid clusters may also chemotax via collective guidance. (a) As the number of cells N in a cluster increases, the mean velocity $\langle V_x \rangle$ increases with N but then saturates. (b) The chemotactic index approaches unity, but more slowly than in a rigid cluster. Rigid cluster theory assumes the same cluster geometries as in Fig. 3. Averages in (a) and (b) are over $n \geq 20$ trajectories (ranging from $n = 20$ for $N = 217$ to $n = 4000$ for $N = 1, 2$), over the time 12.5τ to 50τ . (c) Breakdown of a cluster as it moves up the chemoattractant gradient. X marks the initial cluster center of mass, O the current center. $|\nabla S| = 0.1$, $\bar{\beta} = 1$ in this simulation.

non-gradient-sensing cells via collective guidance through regulation of CIL.

B. A. C. appreciates helpful discussions with Albert Bae and Monica Skoge. This work was supported by NIH Grant No. P01 GM078586, by NSF Grant No. DMS 1309542, and by the Center for Theoretical Biological Physics. B. A. C. was supported by NIH Grant No. F32GM110983.

-
- [1] H. Levine and W.-J. Rappel, The physics of eukaryotic chemotaxis, *Phys. Today* **66**, No. 2, 24 (2013).
- [2] J. E. Segall, S. M. Block, and H. C. Berg, Temporal comparisons in bacterial chemotaxis, *Proc. Natl. Acad. Sci. U.S.A.* **83**, 8987 (1986).
- [3] E. Theveneau, L. Marchant, S. Kuriyama, M. Gull, B. Moepps, M. Parsons, and R. Mayor, Collective chemotaxis requires contact-dependent cell polarity, *Dev. Cell* **19**, 39 (2010).
- [4] G. Malet-Engra, W. Yu, A. Oldani, J. Rey-Barroso, N. S. Gov, G. Scita, and L. Dupré, Collective cell motility promotes chemotactic prowess and resistance to chemorepulsion, *Curr. Biol.* **25**, 242 (2015).
- [5] A. Bianco, M. Poukkula, A. Cliffe, J. Mathieu, C. M. Luque, T. A. Fulga, and P. Rørth, Two distinct modes of guidance signalling during collective migration of border cells, *Nature (London)* **448**, 362 (2007).
- [6] P. Rørth, Collective guidance of collective cell migration, *Trends Cell Biol.* **17**, 575 (2007).
- [7] M. Inaki, S. Vishnu, A. Cliffe, and P. Rørth, Effective guidance of collective migration based on differences in cell states, *Proc. Natl. Acad. Sci. U.S.A.* **109**, 2027 (2012).
- [8] X. Wang, L. He, Y. I. Wu, K. M. Hahn, and D. J. Montell, Light-mediated activation reveals a key role for Rac in collective guidance of cell movement in vivo, *Nat. Cell Biol.* **12**, 591 (2010).
- [9] A. Berdahl, C. J. Torney, C. C. Ioannou, J. J. Faria, and I. D. Couzin, Emergent sensing of complex environments by mobile animal groups, *Science* **339**, 574 (2013).
- [10] B. Lin, T. Yin, Y. I. Wu, T. Inoue, and A. Levchenko, Interplay between chemotaxis and contact inhibition of locomotion determines exploratory cell migration, *Nat. Commun.* **6**, 6619 (2015).
- [11] C. Carmona-Fontaine, H. K. Matthews, S. Kuriyama, M. Moreno, G. A. Dunn, M. Parsons, C. D. Stern, and R. Mayor, Contact inhibition of locomotion in vivo controls neural crest directional migration, *Nature (London)* **456**, 957 (2008).
- [12] R. A. Desai, S. B. Gopal, S. Chen, and C. S. Chen, Contact inhibition of locomotion probabilities drive solitary versus collective cell migration, *J. R. Soc., Interface* **10**, 20130717 (2013).
- [13] A. M. Simons, Many wrongs: The advantage of group navigation, *Trends Ecol. Evol.* **19**, 453 (2004).
- [14] L. Coburn, L. Cerone, C. Torney, I. D. Couzin, and Z. Neufeld, Tactile interactions lead to coherent motion and enhanced chemotaxis of migrating cells, *Phys. Biol.* **10**, 046002 (2013).
- [15] P. Friedl, J. Locker, E. Sahai, and J. E. Segall, Classifying collective cancer cell invasion, *Nat. Cell Biol.* **14**, 777 (2012).
- [16] N. Aceto, A. Bardia, D. T. Miyamoto, M. C. Donaldson, B. S. Wittner, J. A. Spencer, M. Yu, A. Pely, A. Engstrom, H. Zhu *et al.*, Circulating tumor cell clusters are oligoclonal precursors of breast cancer metastasis, *Cell* **158**, 1110 (2014).
- [17] D. Selmececi, S. Mosler, P. H. Hagedorn, N. B. Larsen, and H. Flyvbjerg, Cell motility as persistent random motion: Theories from experiments, *Biophys. J.* **89**, 912 (2005).
- [18] N. G. Van Kampen, *Stochastic Processes in Physics and Chemistry*, Vol. 1 (Elsevier, New York, 1992).
- [19] R. Mayor and C. Carmona-Fontaine, Keeping in touch with contact inhibition of locomotion, *Trends Cell Biol.* **20**, 319 (2010).
- [20] B. A. Camley, Y. Zhang, Y. Zhao, B. Li, E. Ben-Jacob, H. Levine, and W.-J. Rappel, Polarity mechanisms such as contact inhibition of locomotion regulate persistent rotational motion of mammalian cells on micropatterns, *Proc. Natl. Acad. Sci. U.S.A.* **111**, 14770 (2014).
- [21] M. Abercrombie, Contact inhibition and malignancy, *Nature (London)* **281**, 259 (1979).
- [22] See Supplemental Material at <http://link.aps.org/supplemental/10.1103/PhysRevLett.116.098101>, which contains some side notes including cluster rotation, extended derivations, numerical details of the simulation method, and a table of parameters.
- [23] S. Kim and S. J. Karrila, *Microhydrodynamics: Principles and Selected Applications* (Courier Dover Publications, Mineola, New York, 2013).
- [24] Y. Han, A. Alsayed, M. Nobili, J. Zhang, T. C. Lubensky, and A. G. Yodh, Brownian motion of an ellipsoid, *Science* **314**, 626 (2006).
- [25] D. Fuller, W. Chen, M. Adler, A. Groisman, H. Levine, W.-J. Rappel, and W. F. Loomis, External and internal constraints on eukaryotic chemotaxis, *Proc. Natl. Acad. Sci. U.S.A.* **107**, 9656 (2010).
- [26] T. E. Angelini, E. Hannezo, X. Trepap, J. J. Fredberg, and D. A. Weitz, Cell Migration Driven by Cooperative Substrate Deformation Patterns, *Phys. Rev. Lett.* **104**, 168104 (2010).
- [27] T. E. Angelini, E. Hannezo, X. Trepap, M. Marquez, J. J. Fredberg, and D. A. Weitz, Glass-like dynamics of collective cell migration, *Proc. Natl. Acad. Sci. U.S.A.* **108**, 4714 (2011).
- [28] A. Szabó, R. Ünnepe, E. Méhes, W. Tsal, W. Argraves, Y. Cao, and A. Czirók, Collective cell motion in endothelial monolayers, *Phys. Biol.* **7**, 046007 (2010).
- [29] S. R. K. Vedula, A. Ravasio, C. T. Lim, and B. Ladoux, Collective cell migration: A mechanistic perspective, *Physiol. Behav.* **28**, 370 (2013).
- [30] P. B. Warren, Vapor-liquid coexistence in many-body dissipative particle dynamics, *Phys. Rev. E* **68**, 066702 (2003).
- [31] G. Amselem, M. Theves, A. Bae, E. Bodenschatz, and C. Beta, A stochastic description of Dictyostelium chemotaxis, *PLoS One* **7**, e37213 (2012).
- [32] A. Levchenko and P. A. Iglesias, Models of eukaryotic gradient sensing: Application to chemotaxis of amoebae and neutrophils, *Biophys. J.* **82**, 50 (2002).
- [33] K. Takeda, D. Shao, M. Adler, P. G. Charest, W. F. Loomis, H. Levine, A. Groisman, W.-J. Rappel, and R. A. Firtel,

- Incoherent feedforward control governs adaptation of activated Ras in a eukaryotic chemotaxis pathway, *Sci. Signal. (Online)* **5**, ra2 (2012).
- [34] N. Sepúlveda, L. Petitjean, O. Cochet, E. Grasland-Mongrain, P. Silberzan, and V. Hakim, Collective cell motion in an epithelial sheet can be quantitatively described by a stochastic interacting particle model, *PLoS Comput. Biol.* **9**, e1002944 (2013).
- [35] B. A. Camley and W.-J. Rappel, Velocity alignment leads to high persistence in confined cells, *Phys. Rev. E* **89**, 062705 (2014).
- [36] B. Szabo, G. J. Szöllösi, B. Gönci, Z. Jurányi, D. Selmeczi, and T. Vicsek, Phase transition in the collective migration of tissue cells: experiment and model, *Phys. Rev. E* **74**, 061908 (2006).
- [37] B. Li and S. X. Sun, Coherent motions in confluent cell monolayer sheets, *Biophys. J.* **107**, 1532 (2014).
- [38] A. Czirók, E. Ben-Jacob, I. Cohen, and T. Vicsek, Formation of complex bacterial colonies via self-generated vortices, *Phys. Rev. E* **54**, 1791 (1996).
- [39] R. van Dronghelen, A. Pal, C. P. Goodrich, and T. Idema, Collective dynamics of soft active particles, *Phys. Rev. E* **91**, 032706 (2015).
- [40] M. Basan, J. Elgeti, E. Hannezo, W.-J. Rappel, and H. Levine, Alignment of cellular motility forces with tissue flow as a mechanism for efficient wound healing, *Proc. Natl. Acad. Sci. U.S.A.* **110**, 2452 (2013).
- [41] J. Zimmermann, R. L. Hayes, M. Basan, J. N. Onuchic, W.-J. Rappel, and H. Levine, Intercellular stress reconstitution from traction force data, *Biophys. J.* **107**, 548 (2014).
- [42] F. J. Seegerer, F. Thüroff, A. Piera Alberola, E. Frey, and J. O. Rädler, Emergence and Persistence of Collective Cell Migration on Small Circular Micropatterns, *Phys. Rev. Lett.* **114**, 228102 (2015).